HHS Public Access

Author manuscript

Nat Struct Mol Biol. Author manuscript; available in PMC 2012 December 24.

Published in final edited form as:

Nat Struct Mol Biol. ; 19(6): 633–641. doi:10.1038/nsmb.2289.

A glutamate switch controls voltage-sensitive phosphatase function

Lijun Liu[1,4,10], **Susy C. Kohout**[8,10], **Qiang Xu**[1,4,9], **Simone Müller**[1,4], **Christopher R. Kimberlin**[1,4], **Ehud Y. Isacoff**[5,6,7,8], and **Daniel L. Minor Jr.**[1,2,3,4,5]

[1]Cardiovascular Research Institute, University of California, San Francisco, California 94158-2330

[2]Department of Biochemistry and Biophysics, University of California, San Francisco, California 94158-2330

[3]Department of Cellular and Molecular Pharmacology, University of California, San Francisco, California 94158-2330

[4]California Institute for Quantitative Biomedical Research, University of California, San Francisco, California 94158-2330

[5]Physical Biosciences, Lawrence Berkeley National Laboratory, Berkeley, CA 94720 USA

[6]Materials Science Divisions, Lawrence Berkeley National Laboratory, Berkeley, CA 94720 USA

[7]Helen Wills Neuroscience Institute, University of California, Berkeley, CA 94720

[8]Department of Molecular and Cell Biology, University of California, Berkeley, CA 94720

Abstract

Ciona intestinalis voltage sensing phosphatase Ci-VSP couples a voltage-sensing domain (VSD) to a lipid phosphatase similar to the tumor suppressor PTEN. How the VSD controls enzyme function has been unclear. Here, we present high-resolution crystal structures of the Ci-VSP enzymatic domain that reveal conformational changes in a key loop, termed the “gating loop”, that controls access to the active site by a mechanism in which residue Glu411 directly competes with substrate. Structure-based mutations that restrict gating loop conformation impair catalytic function and demonstrate that Glu411 also contributes to substrate selectivity. Structure-guided

Correspondence to should be addressed to D.L.M. (daniel.minor@ucsf.edu)..

[9]Present address: Institute of Nuclear-Agricultural Sciences, Zhejiang University, 310029 Hangzhou, China.

[10]These authors contributed equally to this work.

Accession codes

Coordinates and structure factors have been deposited in the Protein Data Bank with the following accession codes: 241 Form I, 3V0D; 241 Form II, 3V0F; 241 Form III, 3V0G; 241 Δ401-405, 3V0J; 241-IP_3 complex, 3V0H; 256, 3V0E; and 256-E411F, 3V0I.

Author contributions

L.L., S.C.K, S. M., E.Y.I. and D.L.M. conceived the study. L.L., S.C.K., Q.X., S.M., and C.R.K. performed the experiments and analyzed data. E.Y.I. and D.L.M. analyzed data and provided guidance and support throughout. L.L., S.C.K., E.Y.I., and D.L.M. wrote the paper.

Conflict of Interest

The authors declare no conflict of interest.

mutations further define an interaction between the gating loop and linker that connects the phosphatase to the VSD for voltage control of enzyme activity. Together, the data suggest that functional coupling between the gating loop and the linker forms the heart of the regulatory mechanism that controls voltage-dependent enzyme activation.

Introduction

Ci-VSP, the *Ciona intestinalis* voltage-sensing phosphatase, is the founding member of a novel membrane protein family in which a transmembrane voltage-sensing domain (VSD) controls activity of a C-terminal cytoplasmic enzyme domain that has sequence similarity to the tumor suppressor PTEN (protein lipid phosphatase and tensin homologue deleted on chromosome 10) rather than an ion channel pore[1-3]. This VSD-PTEN protein class is found in frogs, fish, mice, and humans[4] and provides a direct means to couple membrane potential changes with phosphatase action[1,5,6]. Despite extensive biophysical characterization, structural underpinnings of how voltage controls Ci-VSP function have remained unclear. Two distinct conceptual models have been forwarded to explain how the VSD response to voltage changes drives enzymatic activity of the cytoplasmic domain: simple movement of active site to the membrane[6] and a voltage-dependent conformational change in the active site[7].

To define elements that influence Ci-VSP function, we determined six Ci-VSP cytoplasmic domain high-resolution X-ray crystal structures of different conformations and variants and one substrate analog complex. These reveal an enzymatic domain loop, the “gating loop”, that differs substantially from its PTEN counterpart, the “TI loop”, and that displays three distinct conformations that open or close active site access by controlling the position of gating loop residue Glu411. Functional investigation of a battery of structure-based mutants evaluated in the isolated enzymatic domain *in vitro* and full-length protein in live cells show that Glu411 contributes to activity. Further, our data suggest that the linker region that connects the VSD to the enzymatic domain and is known to be important for function[6,7], couples voltage-sensing to enzyme activity by controlling gating loop action. Together, the results provide a new model in which gating loop conformational changes play an essential role in how voltage regulates Ci-VSP activity.

Results

Ci-VSP cytoplasmic domain high-resolution structure

We crystallized several Ci-VSP cytoplasmic domain constructs in different conditions and crystal habits (Table 1, Supplementary Fig. 1). The highest resolution diffraction data came from a construct that encompassed the VSD-phosphatase linker and the entire C-terminal cytoplasmic domain (residues 241-576, denoted “241”) bearing the catalytic site mutant, C363S[1], (Form I, Table 1). Molecular replacement with a PTEN-based model showed that 241 Form I crystals contained two essentially identical copies in the asymmetric unit (all atom RMSD = 0.48Å, Supplementary Table 1). Because of the superior electron density, we use copy B for description and comparisons. As anticipated from the PTEN sequence similarity (Fig. 1a), the Ci-VSP cytoplasmic domain (Fig. 1b) comprises an N-terminal

phosphatase domain (residues 263-431) having the canonical phosphatase fold found in Protein Tyrosine Phosphatase 1B, PTP1B[8-11], (Supplementary Fig. 2a) and a C-terminal C2 domain (residues 432-576)[12]. (PTEN RMSD$_{C\alpha}$ = 1.60 Å) (Fig. 1c, Supplementary Table 1).

The Ci-VSP 241 Form I structure revealed three unanticipated differences from PTEN that impact the active site (Fig. 1c). (1) Similar to Matsuda *et al.*[13], the C2 domain β-strand 6-7 loop (Ci-VSP residues 512-526, the "522 loop") is in a different orientation than the corresponding PTEN loop (PTEN residues 259-270, the "CBR3 loop") and contributes Tyr522 to the active site (Fig. 1c, d). (2) The phosphatase domain loop between helices 5 and 6 (residues 398-413, the "gating loop"), which is five residues longer than the homologous TI loop in PTEN (PTEN residues 159-169), adopts a conformation, differing from the lower-resolution Ci-VSP structure[13], that buries Glu411 inside a hydrophobic pocket comprising Gly371, Leu391, Phe394, and Ile416, from α-helices 4, 5, and 6, denoted the "α456 pocket" (Fig. 1c-e). (3) The linker region (residues 241-263) folds as an α-helix followed by a β-hairpin (Fig. 1b, c). The α-helix, absent from previous Ci-VSP structures[13], coincides with the expected C-terminal end of the transmembrane S4 segment and positions residues important for coupling voltage-sensing to activity[6,7], Lys252 and Arg253, near the gating loop and active site, respectively. Differences in gating loop and linker conformations between 241 Form I and the structures of PTEN and a prior Ci-VSP construct[13] suggest that these segments may be mobile and have roles in function.

Multiple Ci-VSP structures reveal gating loop movement

The core regions of the structures of two other 241 C363S crystal forms, Forms II and III, (Table 1, Supplementary Fig. 1b, c) and a C363S construct having a truncated linker domain, denoted "256" (residues 256-576, C363S) (Table 1, Supplementary Fig. 1d) were similar to 241 Form I (Fig. 2a, b, Supplementary Table 1). However, the linker and gating loop had notable differences. The extent of α-helical structure in the linker varied in the three 241 structures whereas the β-hairpin remained. In 256, the visible part of the linker common to 241 and 256 (residues 258-263) had no regular secondary structure (Fig. 2b). The gating loop conformations in 241 Form I and 241 Form III were similar, whereas this region adopted a different conformation in the 241 Form II and 256 structures (Fig. 2c, d).

Further comparison revealed that even though the gating loop N-terminal end showed a range of conformations (Fig. 2a, b), some of which make minor crystal lattice interactions (Supplementary Table 2), a four-residue C-terminal segment (residues 409-412) adopted just two (Fig. 2c, d) that placed Glu411 in either the hydrophobic α456 pocket (241 Forms I and III) (Fig. 2c) or the active site (241 Form II, both chains, and 256) (Fig. 2c, d). This second conformation, similar to that seen by Matsuda *et al*.[13], docks Val410 rather than Glu411 in the α456 pocket (Fig. 2c, d). Having Glu411 in the α456 pocket leaves the active site wide-open ("open") (Fig. 2e), whereas having Glu411 in the active site ("closed") leaves only a small pocket occupied by a sulfate ion in the 256 structure (Fig. 2f) and should preclude substrate binding. Refinement of 241 Form I revealed a minor conformation in which Glu411 has a similar position to that in 256. The reduced active site pocket size in the closed form is striking given prior evidence that a 256 construct bearing a catalytically competent active site is inactive[7]. This, together with the observation of open and closed

conformations, suggests that the conserved gating loop 409-412 segment (Supplementary Fig. 3) forms a switch controlling active site access and catalytic domain activity.

Active site architecture

The Ci-VSP P-loop signature motif (residues His362-Arg369) adopts the canonical structure of protein tyrosine phosphatases[11,14] (Supplementary Figure 2a, b) and PTEN[15] (Fig. 1c, d) and is exceptionally well ordered, having B-factors among the lowest in the structure (Supplementary Fig. 2c-e). The active site pocket is lined by a loop that contributes general acid-base residues for catalysis, (residues 330-333, the "D331 loop") in a conformation identical to PTEN (Fig. 1d). The D331 loop is joined by Tyr522, which closes off a shallow pocket occupied by solvent in PTEN (Fig. 1d, Supplementary Fig. 2f) and whose hydroxyl is oriented in a manner seemingly ideal for substrate interactions. The 241 Form I electron density also revealed a phosphate ion coordinated by Arg369, the P-loop element commonly used to bind substrate phosphates[11] (Fig. 1d). This phosphate position coincides with a sulfate ion in 256 and substrate phosphate in PTP1B phosphatase-substrate complexes[8,16] (Supplementary Fig. 2b). Thus, it likely marks the position of the phosphate that Ci-VSP would cleave from its substrates.

Residues central to the active site, Ser363-Gly366, adopt two distinct conformations (Fig. 3a). The 256 active site matches the Matsuda *et al.* 236 structure[13] (Fig. 3b), whereas, the 241 Form I and Form III active sites match the Matsuda *et al.* G365A mutant[13] (Fig. 3c) and are similar to PTEN, which has an alanine at the 365 equivalent position. The 241 Form II and the Matsuda *et al.* 248 active sites adopt a conformation hybrid between the 241 Form I and 256 structures. These differences are uncorrelated with gating loop status (Supplementary Table 3). Nevertheless, this active site mobility may influence catalysis. Together, the multiple structures point to active site and gating loop conformational changes that we set out to investigate in turn.

Roles of Gly365 and Tyr522 in enzymatic activity

Ci-VSP cleaves the 5-phosphate of $PI(3,4,5)P_3$ and $PI(4,5)P_2$[17-19] and has weaker activity against the 3-phosphate[17]. In contrast, PTEN acts solely on the $PI(3,4,5)P_3$ 3-phosphate[17,20,21]. These specificity differences have been suggested to originate from an Ala→Gly difference at Ci-VSP active site residue 365[4,17]; however, the 241 Form I structure shows that Ci-VSP and PTEN active sites are identical (RMSD = 0.29 Å and 0.77 Å, C_α and all atoms, respectively) (Fig. 1d, Supplementary Table 1). To investigate whether the Ala→Gly difference might affect substrate specificity, we conducted a series of functional assays on full-length Ci-VSP G365A in live *Xenopus* oocyte membranes in the context of a second mutation, G214C, that serves as a fluorescent label attachment site at the S4 transmembrane segment external end to assess membrane expression and VSD conformational changes[5].

We co-expressed Ci-VSP with Kir2.1-R228Q (Kir2.1Q), a potassium channel activated by $PI(4,5)P_2$[1,5,7,18], and used Kir2.1Q activity as a reporter of Ci-VSP-induced changes in $PI(4,5)P_2$ levels. Comparison with wild-type (WT) and the catalytically inactive mutant C363S showed that CiVSP-G365A produces a depolarization-induced reduction of Kir2.1Q

current (Fig. 4a), indicating that the G→A change does not make Ci-VSP an exclusive 3-phosphatase like PTEN.

To test specificity further, we used a set of green fluorescent protein (GFP)-tagged pleckstrin homology (PH) domains that bind to different phosphoinositides: a $PI(4,5)P_2$ probe, phospholipase C (PLC) PH domain (GFP-PLC-PH)[18,19] (Fig. 4b); a $PI(3,4,5)P_3$ probe, general receptor for phosphoinositides-1 (GRP1) PH domain (GFP-GRP-PH) (Fig. 4c); and a $PI(3,4)P_2$ probe, the tandem PH domain-containing protein 1 (TAPP-1) PH domain (GFP-TAPP-PH)[19] (Fig. 4d). For $PI(4,5)P_2$ and $PI(3,4,5)P_3$ probes (Fig. 4b, c), following depolarization, both WT and G365A, but not C363S, caused similar probe mobilization, albeit with different magnitudes, suggesting that WT and G365A have similar substrate selectivity. For the $PI(3,4)P_2$ probe (Fig. 4d), WT caused a fluorescence increase that was followed by a decrease. These changes correspond to the probe moving to the membrane because of $PI(3,4)P_2$ generation from $PI(3,4,5)P_3$, and then away from the membrane, indicating $PI(3,4)P_2$ destruction. In contrast, only a small fluorescence decrease was observed with G365A, indicating preservation of some 3-phosphatase activity against $PI(3,4)P_2$. Consistent with prior work[17], all assays showed that G365A has reduced activity relative to WT as indicated by smaller ΔF amplitudes. This reduction is consistent with the idea that active site flexibility is important and is restricted by the introduction of the sidechain methyl group.

To test whether Tyr522 influences Ci-VSP function, we examined the Y522A mutant. Measurements of Kir2.1Q current (Fig. 4a) and depolarization induced membrane fluorescence changes for the $PI(4,5)P_2$ probe (Fig. 4b) indicated that Y522A had little effect on $PI(4,5)P_2$ 5-phosphate dephosphorylation. However, Y522A produced a striking augmentation in the depolarization-induced fluorescence of the $PI(3,4)P_2$ probe (Fig. 4d inset, Supplementary Fig. 4a, b), indicating increased $PI(3,4)P_2$ accumulation. Additionally, Y522A eliminated the transient nature of the rise (Fig. 4d inset, Supplementary Fig. 4b). Such behavior suggests that Y522A slows dephosphorylation at the $PI(3,4)P_2$ 3-phosphate.

We used a malachite green assay[1,7,17] to measure activity of purified WT and Y522A 241 cytoplasmic domain constructs against $PI(3,4,5)P_3$ and $PI(3,4)P_2$. Circular dichroism showed that Y522A does not cause a loss of structure (Supplementary Fig. 4c). Y522A modestly reduced steady-state activity against $PI(3,4)P_2$ relative to WT, but without a significant effect on V_{max} (Fig. 4e; Supplementary Fig. 4d; Supplementary Table 3), indicating no major change to the isolated enzyme fragment substrate specificity. However, Y522A accelerated VSD activation and deactivation rearrangements in voltage-clamp fluorometry (VCF) measurements of tetramethyl-rhodamine-maleimide (TMRM) labeled full-length protein (Fig. 4f). This is reminiscent of how other catalytic site mutations affect VSD motion[6,7,18] and together with the effects on GFP-probe behavior supports the idea that Tyr522 has a role in Ci-VSP function.

Gating loop conformation and Ci-VSP function

To address the hypothesis that gating loop mobility plays a role in controlling enzyme activity, we made a set of Glu411 hydrophobic substitutions (E411L, I, and F) that should favor residue 411 occupancy of the hydrophobic α456 pocket and stabilize the open

conformation. We also made a deletion (Δ401-405) that removed gating loop residues having the greatest structural variation to create a Ci-VSP gating loop of equal length to the PTEN TI loop (Fig. 5a).

Malachite green assays showed that all three hydrophobic mutants reduced PI(3,4,5)P_3 dephosphorylation (Fig. 5b) with E411F causing the biggest reduction. Δ401-405 resulted in a near complete loss of activity (Fig. 5b). All three Glu411 hydrophobic mutants and Δ401-405 eliminated activity of full-length Ci-VSP measured in oocytes using the Kir2.1Q reporter assay (Fig. 5c). In contrast, polar substitutions (E411D, Q, and T) had a milder impact on the isolated enzymatic domain and full-length protein (Fig. 5b, c).

We determined the structures of the two gating loop mutants that caused the most dramatic functional losses, E411F and Δ401-405 (Table 1, Fig. 5d-g). E411F crystallized in a 256 background that bore a native active site residue Cys363, whereas Δ401-405 crystallized in the 241 C363S background. The overall structures of 256-E411F and 241 Δ401-405 are very similar to the 256 and 241 Form I structures, respectively (Supplementary Table 1). The similarity of 256-E411F to the other structures demonstrates that, as expected from phosphatase structural studies[8], the C363S mutation has a negligible impact on conformation.

In the E411F-256 structure, the gating loop segment is in the open conformation having E411F in the hydrophobic α456 pocket (Fig. 5e, Supplementary Table 2). In contrast, the Δ401-405 structure shows that the gating loop N-terminal deletion yields a closed conformation (Fig. 5f, Supplementary Table 2). Both structures have a catalytic site conformation identical to that of 241 Form I, providing additional evidence that the conformation of this region and the gating loop are uncorrelated (Supplementary Table 3). Notably, neither gating loop conformation matches the equivalent PTEN region in which Thr167, the 411 counterpart, is midway between open and closed conformations (Fig. 5g). This, together with the functional data showing that E411F (open) and Δ401-405 (closed) dramatically impair activity of the isolated domain and full-length protein (Fig. 5b, c), suggests that the structures represent trapped forms of two key 410-412 segment conformations. The structures further suggest that gating loop movement, centered on the exchange of residues 410 and 411 in the α456 hydrophobic pocket, is part of the Ci-VSP catalytic cycle.

To probe the gating loop further, we examined E411T and E411F in the full-length protein expressed in *Xenopus* oocytes using the GFP-PH domain assay and VCF. E411F did not generate detectable PI(3,4)P_2 (Fig. 5h). In contrast, E411T caused an unexpected increase in GFP-TAPP-PH membrane fluorescence that lacked the subsequent late declining phase seen with WT (Fig. 5h). This was accompanied by a slowing of the fluorescence increase (Supplementary Figure 4a, b), suggesting that E411T moderately slows PI(3,4,5)P_3 5-phosphate dephosphorylation and strongly decreases PI(3,4)P_2 3-phosphate dephosphorylation. Kinetic studies on the isolated cytosolic domain confirmed the decrease in 3-phosphate dephosphorylation, showing a two-fold reduction in V_{max} for the E411T cytosolic domain relative to WT (Supplementary Figure 4d, Supplementary Table 4). VCF measurements showed that both E411T and E411F altered VSD movement (Fig. 5i). E411T

shifted the activation curve to the left (-13.2 mV), and slowed deactivation, suggesting active state stabilization. Conversely, E411F shifted the activation curve to the right (+11.3 mV) and slightly accelerated deactivation, consistent with resting state stabilization. Together, the sensitivity to changes at Glu411 supports the idea that gating loop motion is crucial to Ci-VSP function and suggests that Glu411 may have a role in substrate recognition.

A gating loop conformation similar to PTEN

The structure of a complex of a soluble substrate mimic, myo-inositol-1,4,5-trisphosphate (IP_3) and the 241 C363S construct (Table 1) revealed an IP_3 molecule in the active site (Fig. 6a, b) and a gating loop in which Glu411 is between the open and closed positions (Fig. 6c). Here, Val410 remains in the α456 pocket (Fig. 6d) and the active site conformation identical to 241 Form I (Supplementary Table 3). The active site IP_3 clashes sterically with the Glu411 closed conformation (Fig. 6b-d) and provides direct evidence that the gating loop must move to accommodate substrate binding. The remainder of the gating loop is very similar to the closed 241 Form II chain B. Strikingly, the Val410 and Glu411 conformations are exceptionally similar to the equivalent PTEN positions, including alignment of Ci-VSP Glu411 and PTEN Thr167 across the Cα-Cγ positions (Fig. 6d).

The IP_3 has its 1-phosphate at the position of the active site phosphate and sulfate from the 241 and 256 structures, respectively, (Fig. 6a). In native Ci-VSP inositol phosphate substrates, the 1-phosphate links the inositol ring to a lipid and thus, is unlikely to be cleaved. Nevertheless, a counterclockwise rotation of the IP_3 can be made to place the 5-phosphate in the active site and 4-phosphate in a position where it could interact with Glu411.

The structure also revealed a second IP_3 bound to cationic residues, proximal to the active site, Arg281, Arg286, Arg313, and Lys364, (Supplementary Fig. 5). As this region is likely to appose the lipid bilayer, this second IP_3 site may represent a position for nonspecific interactions with the membrane or may have a more specific role in affecting substrate movement into or out of the active site.

Gating loop-linker coupling

To probe how voltage changes drive Ci-VSP function, we investigated the linker-gating loop relationship. Inspection of the N-terminal linker in 241 Form I, where this element is most completely defined, (Fig. 7a) suggested residues that might mediate gating loop-linker coupling: the conserved gating loop residues 398-400 (Supplementary Fig. 3) and linker residues Lys252 and Arg253, known to couple voltage changes to activity[6,7]. In 241 Form I, gating loop Asp400 interacts via a salt bridge with Lys252 and linker residue Arg253 coordinates the Gly365 backbone carbonyl of the active site. Notably, Lys252 and Arg253, exchange positions between the 241 Form I and IP_3 bound structures (Fig. 7b). Lys252 goes from a solvent-exposed interaction with Asp400 to a position that makes a hydrogen bond to the Gly365 carbonyl. Conversely, Arg253 goes from coordinating the Gly365 carbonyl to a solvent exposed interaction with Asp400. This exchange is also present in the closed structure 241 Form II chain B (Supplementary movie). Gating loop Arg398 makes hydrogen

bond interactions with the active site loop (Fig. 7a) in all of the structures. Based on the structures and evidence that K252Q and R253Q drastically reduce voltage-dependent activity and uncouple the VSD from the active site[7], we changed Asp400 to Asn, Ala, Lys, and Arg. All were detrimental to enzymatic domain (Fig. 7c) and full-length protein function (Fig. 7d). None affected the structure as assessed by circular dichroism (Supplementary Fig. 6).

We next asked if Asp400 has a role in coupling the VSD and active site. Earlier analysis of this kind showed that linker residues Lys252 and Arg253 are critical for voltage dependent activity and for coupling catalytic site properties to the VSD[7]. Asp400 mutants that abolished enzymatic domain activity, D400K and D400R, almost eliminated the dramatic influence of a catalytic site mutation, D311A on VSD deactivation rate, consistent with disruption of VSD-active site coupling (Fig. 7e). Together, the data suggest that voltage-dependent rearrangements of the VSD couple to the enzyme active site via interactions between linker residues Lys252 and Arg253 and their gating loop partner Asp400.

Discussion

Understanding how transmembrane voltage changes influence the activity of diverse membrane proteins remains a challenge[22]. In voltage-gated phosphatases two distinct models could explain how membrane depolarization regulates membrane lipid dephosphorylation. In one, analogous to the PTEN diffusion-based process where the N-terminal domain interacts with the membrane, depolarization would cause the Ci-VSP linker to interact with membrane phospholipids and place a constitutively active catalytic site within reach of substrate[6]. In a second model, depolarization would drive a conformational change that gates the catalytic activity[7]. Our studies strongly support the second.

The crystal structures show that gating loop residues 409-412 form a switch that adopts three distinct conformations: open, closed, and bound. Gating loop movement between the open and closed is dramatic (Supplementary movie). Glu411 moves from a hydrophobic cavity formed by the α4, α5, and α6 helices in the open state into the active site in the closed state, where it is in direct steric competition with substrate. Repositioning Glu411 to the bound conformation, which overlaps remarkably well with the analogous PTEN TI loop, relieves the direct steric competition between Glu411 and substrate in the closed form (Fig. 6). Thus, gating loop movement is a central aspect of Ci-VSP function. These conformational changes may account entirely for voltage dependent regulation of activity, but may also be accompanied by active site movement relative to the membrane.

Two mutants dramatically demonstrate the importance of Ci-VSP gating loop movement for function. Ci-VSP Δ401-405, having the gating loop truncated to a PTEN-equivalent length, is inactive due to Glu411 active site occupation. Conversely, E411F favors the open gating loop conformation and a wide-open active site similar to PTEN (Fig. 5d, e). This arrangement should offer unfettered substrate access to the active site and yet, disrupts Ci-VSP function (Fig. 5b, c). This seeming paradox suggests that the gating loop does more than simply control active site access. Indeed, E411T influences both substrate selectivity and VSD movement (Fig. 5h,i). Thus, the data point to a mechanism in which the gating

loop facilitates active site entry or exit of substrate, product, or both, and underscore a central role for Glu411 in this process.

Burial of a glutamate in a hydrophobic cavity, as seen with Glu411 in the α456 pocket, is unusual, but not unprecedented[23,24]. There are well-characterized examples where hydrophobic pockets interact with charged or polar ligands[25-27]. Nevertheless, such interactions have an energetic penalty that is likely to be an important component of gating loop function. Indeed, Glu411→hydrophobic mutations, which should partition into the α456 hydrophobic cavity, drastically reduce activity (Fig. 5b, c). This result fits with the concept of a tradeoff between stability and function for enzymatic residues involved in substrate binding and catalysis[28] and suggests that gating loop mobility depends on the hydrophilic character of residue 411.

Our findings also highlight the interdomain linker connecting the VSD and enzyme[1,6,7]. Structure-based mutational analysis indicates that two linker residues, Lys252 and Arg253, and gating loop residue Asp400 are key to linker-gating loop coupling. This is substantially different from the PTEN[29-31] membrane recruitment mechanism[6] and instead supports a mechanism driven by voltage-dependent conformational change in the active site[7]. Notably, the structural plasticity of the gating loop N-terminal end contrasts with the switch region conformational properties. Interactions of this portion of the gating loop with the lipid bilayer, absent from the structures, may be important for mediating VSD-switch region coupling.

The data presented here uncover a previously unknown element required for Ci-VSP function, the “gating loop”. The gating loop switch region, residues 409-412, adopts three distinct conformations that we propose are part of the catalytic cycle (Fig. 7f), in which substrate is given active site access (open), occluded from the active site (closed), or selected (bound) by Glu411. The ability of the gating loop to access these conformations is controlled by the VSD and involves linker residues Lys252 and Arg253 and gating loop residue Asp400. Together, the results suggest that a mobile gate whose conformation is modulated by the linker that connects the cytoplasmic domain to the voltage-sensing S4 segment of the VSD mediates the voltage dependence of Ci-VSP enzyme activity.

Online methods

Constructs and protein expression

Structural and *in vitro* activity studies used two backgrounds, Ci-VSP 241-576 and 256-576, denoted “241” and “256”, respectively, cloned into pET-28b(+) using NdeI and HindIII to yield a fusion bearing an N-terminal His_6-tag and TEV protease site. Proteins were expressed in *Escherichia coli* Rosetta (DE3) pLysS in 2×YT at 250 rpm and grown to OD_{600} = 0.8 at 37°C, moved to 22°C, and induced with 0.5 mM final concentration isopropyl-β-D-thiogalactopyranoside (IPTG) (EMD Chemicals). Cultures were shaken at 180 rpm, 22°C overnight, harvested (6000×g), frozen in liquid nitrogen and stored at −80°C.

Protein purification

Cells from a 4L growth were sonicated in 100 ml of lysis buffer (50 mM NaCl, 1 mM DTT, 10% glycerol, 30 mM imidazole, 1 mM PMSF, 25 μg ml^{-1} DNAse, 5 mM $MgCl_2$, 20 μg ml^{-1} lysozyme, and 0.05% Triton X-100, 10 mM HEPES pH 7.4,). After centrifugation (40,000×g), supernatant was incubated with 5 ml of Talon Co^{2+} resin (Clontech) 1 hour on a rotary shaker, 4°C. Resin was packed into a column and washed with 100 ml buffer A (50 mM NaCl, 30 mM imidazole, 10 mM HEPES, pH 7.4,), followed by 100 ml buffer B (buffer A plus 450 mM NaCl), and 50 ml buffer A. Protein was eluted with 30 ml stepwise increments of 50 mM and 300 mM imidazole in buffer A. 1 ml of 500 mM EDTA (pH 8.0) was added to the Ci-VSP fraction (300 mM imidazole), and dialyzed overnight (Amicon, MWCO 10,000) against 4 L of buffer C (50 mM NaCl, 3 mM DTT, 50 mM Tris, pH 8.0). For crystallization, TEV protease was added into samples in buffer C during the dialysis at a molar ratio of TEV:Ci-VSP = 1:5 at 4°C overnight with slow rocking. Samples were centrifuged (30,000×g) to remove precipitates, loaded onto Hi-load Q sepharose (256 constructs) or Hi-load SP sepharose (241 constructs) (GE Healthcare) and eluted using a 0-70% gradient of buffer C and buffer D (buffer C + 950 mM NaCl). Ci-VSP fractions were pooled, concentrated to less than 1 ml by Centriprep or Centricon (Amicon, 10,000 MWCO) and run on a Superdex 200 column in buffer C. Ci-VSP fractions were pooled and concentrated to 10 mg ml^{-1} for crystallization. Concentrations were determined by absorbance[32]. For circular dichroism (CD), protein was exchanged into CD buffer (10 mM Na phosphate, pH 7.3, 50 mM NaCl, 3 mM DTT) by passage over a Superdex 200 column (GE Healthcare). All proteins gave single bands on SDS-PAGE and single, monodisperse gel filtration peaks.

Circular dichroism

Circular dichroism spectra were measured on an Aviv model 215 spectrometer (Aviv Biomedical) from 300 nm to 200 nm at 4°C using a 0.1 cm path length cuvette. Five scans of the same sample were averaged. Molar ellipticity was calculated as: $[\Theta]= 100(m)/Cnl$, where m is the CD signal in millidegrees, C is protein concentration in millimolar, n is the number of residues, and l is path length in centimeters.

In vitro phosphatase assay

Chloroform:methanol:water (1:2:0.8) solutions of 1,2-dioleoyl-sn-glycero-3-phospho-L-serine (PS) and either 1,2-dioleoyl-sn-glycero-3-phospho-(1-myo-inositol-3,4,5-trisphosphate), ($PI(3,4,5)P_3$) or 1,2-dioleoyl-sn-glycero-3-phospho-(1-myo-inositol-3,4-trisphosphate), ($PI(3,4)P_2$) lipids (Avanti Polar Lipids) were prepared as described previously [7]. Final concentrations were 150 or 250 μM for $PI(3,4,5)P_3$ or $PI(3,4)P_2$ and 750 μM or 1.25 mM for PS. Steady state reactions were initiated by vesicle addition (40 μl at 75 μM $PI(3,4,5)P_3$) to purified Ci-VSP (10 μl at 2.44 μM), incubated at 25°C and stopped by addition of 50 μl of 100 mM N-ethylmaleimide. Phosphate was measured with the Malachite Green Phosphate Assay Kit (Cayman). Stopped reactions were centrifuged. 50 μl was transferred to a 96 well plate. 5 μl of MG acidic solution was added per well, gently mixed by tapping and incubated at room temperature for 10 minutes. 15 μl of MG blue solution was added per well and gently mixed by tapping and incubated at room temperature for 20

minutes to develop color. Absorption was determined at 620 nm with an Infinite 200 PRO microplate reader (Tecan). Phosphate concentrations were determined by comparison to a KH_2PO_4 standard curve. Reaction with lipids alone was used as control. Kinetic reactions were measured at substrate concentrations of 10, 20, 30, 40, 50, 100, 150 and 200 μM over an 80 minute time period using the Biomol Green reagent (Biomol International, ENZO). Initial velocities were fit for each concentration and plotted versus substrate concentration. Velocity versus substrate plots were fit with V= (Vmax * [S])/(Km +[S]).

Crystallization and Data Collection

Hanging drop crystallization screens (Hampton Research and Qiagen) were done using a Mosquito (TTP Labtech) and optimized with Limbo plates (Hampton Research). 256 crystals were obtained from 2.1-2.3 M ammonium sulfate, 0.1 M HEPES, pH 7.0-7.5. 256-E411F crystals were obtained in a similar condition with 2.5 M ammonium sulfate. 241 Form I and Δ401-405, crystals were grown with 17.5-22.5% PEG 2000, 0.1 M ammonium dihydrophosphate, 0.1 M Tris-HCl, pH 8.0. 241 Form II crystals were obtained by soaking 241 Form I crystals in 25% PEG 2000, 0.1 M Tris-HCl, pH 8.0 by six serial dilutions over three days. 241 Form III crystals of were obtained by soaking Form I crystals in 30% PEG 2000, 0.1 M ammonium dihydrophosphate, 0.1 M Tris-HCl, pH 8.0 overnight. 241-IP_3 complex crystals were prepared by soaking 241 (Form II) in 25% PEG 2000, 0.1 M Tris-HCl, pH 8.0, 2.5 mM IP_3 for three days.

Diffraction data were collected at 100K from crystals flash frozen in liquid nitrogen, Beamline 8.3.1 (ALS, Berkeley, CA), by oscillation at λ= 1.116 Å with an ADSC Quantum 315r detector. For cryo-protection, crystals were passed through their corresponding well solution with addition of 18% glycerol for ammonium sulfate conditions or with PEG 2000 concentrations increased to 30% for PEG 2000 conditions. Data were processed using HKL2000[33].

Structural determination and refinement

Structures were determined by molecular replacement using MolRep[34] and PTEN (PDB code: 1D5R[15]) with non-conserved residues replaced by to alanine as a search model for the solution of 241 Form I and 256. 241 Form I and 256 structures were used for the other crystal forms, depending on the beginning residues. COOT[35] was used for graphical modeling. Structures were refined with Refmac[34], and randomly selected 5% of data were used for R_{free}. Typically, after the molecules were located in the asymmetric unit cell, rigid-body refinement was conducted at 3.5 Å (this refinement was re-performed later as needed), followed by restrained refinement. TLS refinement was applied. For resolution better than 1.5 Å, B factors were refined anisotropically; for the 241 Form I dataset, unrestrained refinement was performed at the end.

Molecular biology for full-length assays

Ci-VSP in the pSD64TF vector was provided by Y. Okamura (Osaka University). GFP-PLC-PH, GFP-TAPP-PH, GFP-GRP-PH were provided by T. Meyer (Stanford University), T. Balla (NIH), and J. Falke (U Colorado), respectively. Each was subcloned into pGEMHE. Kir2.1 was provided by E. Reuveny (Weizmann Institute of Science). Mutations were made

by QuikChange (Stratagene) and confirmed by sequencing. RNA was transcribed using T7 and SP6 mMessage mMachine (Ambion) kits.

Voltage clamp fluorometry

VCF was performed as described previously[7]. Briefly, *Xenopus laevis* oocytes were injected with 50 nl mRNA at 0.02-2.0 mg ml^{-1} depending on the experiment. Cells were then incubated in ND-96 (96 mM NaCl, 2 mM KCl, 1.8 mM $CaCl_2$, 1 mM $MgCl_2$, 50 μg ml^{-1} gentamicin, 2.5 mM Na pyruvate and 5 mM HEPES, pH 7.6) at 18 °C for 24-48 h. Light was filtered through the following filter sets (excitation and emission, respectively): HQ535/50, HQ610/75 for tetramethylrhodamine-6-maleimide (TMRM) and HQ 450/50, HQ510/50 for GFP (Chroma Technology).

On the day of the experiment, cells were treated as described previously[7]. Recording solution was a modified ND-96, ND-96′ (without the gentamicin or pyruvate). Cells were constantly perfused with ND-96′ for all experiments.

Fluorescence measures of activity

RNA ratios of 2:1 (μg μl^{-1}) were used for Ci-VSP and each PH domain (total RNA ~1.2 μg μl^{-1}). Cells were recorded in perfused ND-96′. GFP-PLC-PH, GFP-GRP-PH, and GFP-TAPP-PH were used to detect $PI(4,5)P_2$, $PI(3,4,5)P_3$, and $PI(3,4)P_2$, respectively. For GRP and TAPP PH domains, 8 μM insulin was added to the ND-96′ to promote PI3K activity and boost $PI(3,4,5)P_3$ levels. Catalytically inactive Ci-VSP C363S showed TAPP-PH domain background activity, presumed to come from the native *Xenopus* VSP, Xl-VSP[36]. Therefore, we subtracted an average trace from 19 oocytes expressing C363S from the traces from oocytes expressing WT and mutant Ci-VSP. Because PLC and GRP PH domain recordings showed minimal background activity, they were not corrected. Ci-VSP expression levels were confirmed in each oocyte by TMRM labeling and measurement of the TMRM fluorescence change induced by VSD motion. Other conditions were the same as for the TMRM VCF.

Electrophysiological measures of activity

Ci-VSP catalytic activity was measured by detecting Kir2.1 R228Q (Kir2.1Q) activation by $PI(4,5)P_2$[5]. The cell was hyperpolarized to −100 mV where Ci-VSP is off until a steady state current was established (5-7 minutes) followed by depolarization to +60 mV to activate Ci-VSP until a steady state was re-established (2-7 minutes). Resulting current changes between the Ci-VSP off and on states were measured and expressed as percent activity. Currents were leak subtracted by assuming a voltage-independent linear leak. Current was measured at −100 mV after the test holding potential, and leak was measured at +50 mV where the Kir2.1Q channels should be blocked. Leak-subtracted (LS) current was calculated as: $I_{ls} = I_{-100mV} + 2I_{+50mV}$. Percent activity was calculated as $\Delta I/I_{max} = (I_{+60mV\ first} - I_{+60mVlast})/I_{+60mV\ first}$. 50 nl of mRNA was injected into *X. laevis* oocytes at a 40:1 to a 100:1 (μg μl^{-1}) Ci-VSP:Kir2.1Q (total RNA ~0.9-2 μg μl^{-1}). Ci-VSP expression levels were confirmed using TMRM labeling. Cells were incubated in ND-96 at 18°C for 24-36 h. Recording solutions contained 90 mM K methanesulfonic acid, 3 mM $MgCl_2$, 2 mM $CaCl_2$, 10 mM HEPES, pH 7.4. Other conditions were the same as for VCF.

Data analysis

Kinetic and steady state traces were analyzed using Clampfit (Molecular Devices), IGOR Pro (WaveMetrics, Inc) and Excel (Microsoft) software. Steady state voltage-dependent traces were fit with Boltzmann equations. Data were normalized to the amplitude of the Boltzmann fits. Error bars indicate the S.E.M. Statistical significance was determined using the Student's *t*-test.

Supplementary Material

Refer to Web version on PubMed Central for supplementary material.

Acknowledgements

This work was supported by grants to D.L.M. from NIH, R01 DC007664 and the American Heart Association 0740019N and to E.Y.I. from NIH, R01 NS35549 and U24 NS057631. We thank members of the Minor and Isacoff labs for support throughout these studies. D.L.M. is an AHA Established Investigator.

References

1. Murata Y, Iwasaki H, Sasaki M, Inaba K, Okamura Y. Phosphoinositide phosphatase activity coupled to an intrinsic voltage sensor. Nature. 2005; 435:1239–43. [PubMed: 15902207]
2. Okamura Y, Murata Y, Iwasaki H. Voltage-sensing phosphatase: actions and potentials. J Physiol. 2009; 587:513–20. [PubMed: 19074969]
3. Worby CA, Dixon JE. Phosphoinositide phosphatases: emerging roles as voltage sensors? Mol Interv. 2005; 5:274–7. [PubMed: 16249522]
4. Okamura Y, Dixon JE. Voltage-sensing phosphatase: its molecular relationship with PTEN. Physiology (Bethesda). 2011; 26:6–13. [PubMed: 21357898]
5. Kohout SC, Ulbrich MH, Bell SC, Isacoff EY. Subunit organization and functional transitions in Ci-VSP. Nat Struct Mol Biol. 2008; 15:106–8. [PubMed: 18084307]
6. Villalba-Galea CA, Miceli F, Taglialatela M, Bezanilla F. Coupling between the voltage-sensing and phosphatase domains of Ci-VSP. J Gen Physiol. 2009; 134:5–14. [PubMed: 19564425]
7. Kohout SC, et al. Electrochemical coupling in the voltage-dependent phosphatase Ci-VSP. Nat Chem Biol. 2010; 6:369–75. [PubMed: 20364128]
8. Jia Z, Barford D, Flint AJ, Tonks NK. Structural basis for phosphotyrosine peptide recognition by protein tyrosine phosphatase 1B. Science. 1995; 268:1754–8. [PubMed: 7540771]
9. Barford D, Flint AJ, Tonks NK. Crystal structure of human protein tyrosine phosphatase 1B. Science. 1994; 263:1397–404. [PubMed: 8128219]
10. Andersen JN, et al. Structural and evolutionary relationships among protein tyrosine phosphatase domains. Mol Cell Biol. 2001; 21:7117–36. [PubMed: 11585896]
11. Tabernero L, Aricescu AR, Jones EY, Szedlacsek SE. Protein tyrosine phosphatases: structure-function relationships. FEBS J. 2008; 275:867–82. [PubMed: 18298793]
12. Lemmon MA. Membrane recognition by phospholipid-binding domains. Nat Rev Mol Cell Biol. 2008; 9:99–111. [PubMed: 18216767]
13. Matsuda M, et al. Crystal Structure of the Cytoplasmic Phosphatase and Tensin Homolog (PTEN)-like Region of Ciona intestinalis Voltage-sensing Phosphatase Provides Insight into Substrate Specificity and Redox Regulation of the Phosphoinositide Phosphatase Activity. J Biol Chem. 2011; 286:23368–77. [PubMed: 21543329]
14. Denu JM, Stuckey JA, Saper MA, Dixon JE. Form and function in protein dephosphorylation. Cell. 1996; 87:361–4. [PubMed: 8898189]
15. Lee JO, et al. Crystal structure of the PTEN tumor suppressor: implications for its phosphoinositide phosphatase activity and membrane association. Cell. 1999; 99:323–34. [PubMed: 10555148]

16. Sarmiento M, et al. Structural basis of plasticity in protein tyrosine phosphatase 1B substrate recognition. Biochemistry. 2000; 39:8171–9. [PubMed: 10889023]
17. Iwasaki H, et al. A voltage-sensing phosphatase, Ci-VSP, which shares sequence identity with PTEN, dephosphorylates phosphatidylinositol 4,5-bisphosphate. Proc Natl Acad Sci U S A. 2008; 105:7970–5. [PubMed: 18524949]
18. Murata Y, Okamura Y. Depolarization activates the phosphoinositide phosphatase Ci-VSP, as detected in Xenopus oocytes coexpressing sensors of PIP2. J Physiol. 2007; 583:875–89. [PubMed: 17615106]
19. Halaszovich CR, Schreiber DN, Oliver D. Ci-VSP is a depolarization-activated phosphatidylinositol-4,5-bisphosphate and phosphatidylinositol-3,4,5-trisphosphate 5′-phosphatase. J Biol Chem. 2009; 284:2106–13. [PubMed: 19047057]
20. Maehama T, Dixon JE. PTEN: a tumour suppressor that functions as a phospholipid phosphatase. Trends Cell Biol. 1999; 9:125–8. [PubMed: 10203785]
21. Maehama T, Taylor GS, Dixon JE. PTEN and myotubularin: novel phosphoinositide phosphatases. Annu Rev Biochem. 2001; 70:247–79. [PubMed: 11395408]
22. Bezanilla F. How membrane proteins sense voltage. Nat Rev Mol Cell Biol. 2008; 9:323–32. [PubMed: 18354422]
23. Isom DG, Cannon BR, Castaneda CA, Robinson A, Garcia-Moreno B. High tolerance for ionizable residues in the hydrophobic interior of proteins. Proc Natl Acad Sci U S A. 2008; 105:17784–8. [PubMed: 19004768]
24. Yerushalmi H, Schuldiner S. An essential glutamyl residue in EmrE, a multidrug antiporter from Escherichia coli. J Biol Chem. 2000; 275:5264–9. [PubMed: 10681497]
25. Liu L, Baase WA, Michael MM, Matthews BW. Use of stabilizing mutations to engineer a charged group within a ligand-binding hydrophobic cavity in T4 lysozyme. Biochemistry. 2009; 48:8842–51. [PubMed: 19663503]
26. Zheleznova EE, Markham PN, Neyfakh AA, Brennan RG. Structural basis of multidrug recognition by BmrR, a transcription activator of a multidrug transporter. Cell. 1999; 96:353–62. [PubMed: 10025401]
27. Muth TR, Schuldiner S. A membrane-embedded glutamate is required for ligand binding to the multidrug transporter EmrE. EMBO J. 2000; 19:234–40. [PubMed: 10637227]
28. Shoichet BK, Baase WA, Kuroki R, Matthews BW. A relationship between protein stability and protein function. Proc Natl Acad Sci U S A. 1995; 92:452–6. [PubMed: 7831309]
29. Iijima M, Huang YE, Luo HR, Vazquez F, Devreotes PN. Novel mechanism of PTEN regulation by its phosphatidylinositol 4,5-bisphosphate binding motif is critical for chemotaxis. J Biol Chem. 2004; 279:16606–13. [PubMed: 14764604]
30. Rahdar M, et al. A phosphorylation-dependent intramolecular interaction regulates the membrane association and activity of the tumor suppressor PTEN. Proc Natl Acad Sci U S A. 2009; 106:480–5. [PubMed: 19114656]
32. Edelhoch H. Spectroscopic determination of tryptophan and tyrosine in proteins. Biochemistry. 1967; 6:1948–54. [PubMed: 6049437]
33. Otwinowski Z, Minor W. Processing of X-ray diffraction data collected in oscillation mode. Meth. Enzy. 1997; 276:307–326.
34. Collaborative Computational Project, N. The CCP4 suite: Programs for protein crystallography. Acta Crystallogr D Biol Crystallogr. 1994; 50:760–763. [PubMed: 15299374]
35. Emsley P, Cowtan K. Coot: model-building tools for molecular graphics. Acta Crystallogr D Biol Crystallogr. 2004; 60:2126–32. [PubMed: 15572765]
36. Ratzan WJ, Evsikov AV, Okamura Y, Jaffe LA. Voltage sensitive phosphoinositide phosphatases of Xenopus: their tissue distribution and voltage dependence. J Cell Physiol. 2011

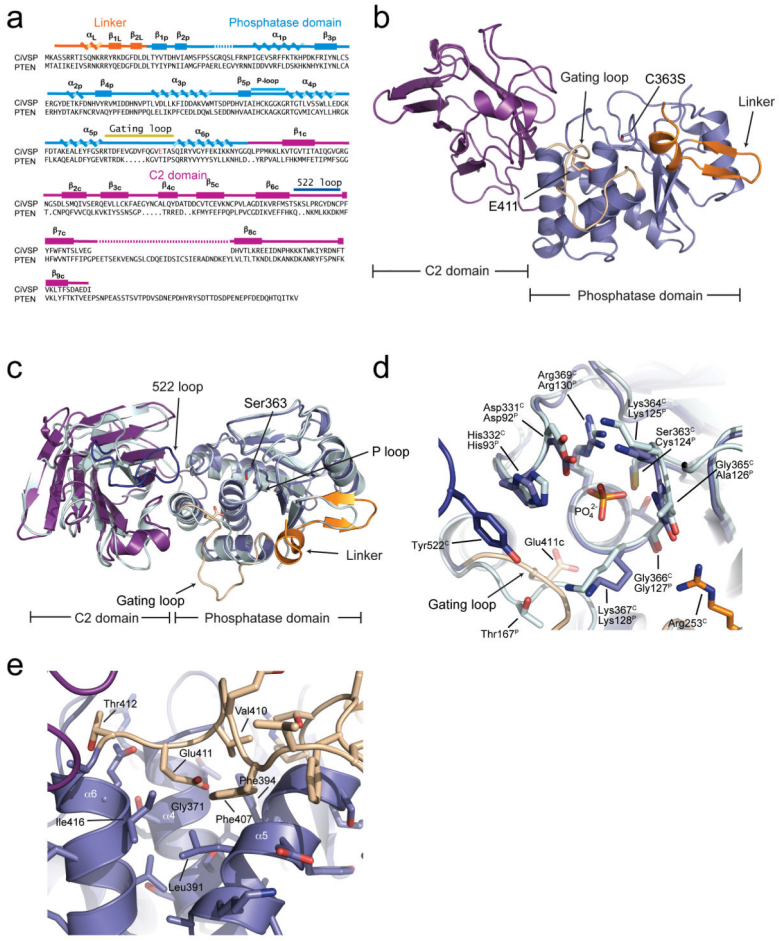

Figure 1.

Structure of the Ci-VSP catalytic domain and comparison with PTEN. (**a)** Ci-VSP intracellular domain (241-576) and PTEN sequence comparison. Secondary structure elements from 241 Form I are indicated. Linker, phosphatase, and C2 domains are orange, slate, and purple, respectively. P-loop and gating loop are indicated by light blue and tan, respectively. Dashed lines indicate residues not modeled or sequence alignment gaps. (**b**) 241 Form I Ci-VSP intracellular domain ribbon diagram. Domains and elements are labeled and colored as follows: N-terminal linker (orange), phosphatase domain (slate), gating loop (tan), C2 domain (purple). C363S and Glu411 are shown as sticks. (**c**)**,** Superposition of Ci-VSP 241 Form I (colored as in panel **b** with the 522 loop shown in dark blue) and PTEN (light blue). (**d**) Structural comparison of Ci-VSP 241 and PTEN active sites. Superscript indicates origin: “C” Ci-VSP and “P” PTEN. Orientation is similar to panel **c**. (**e**) View of the α456 pocket. View is 90° to the orientation in panels **c** and **d**.

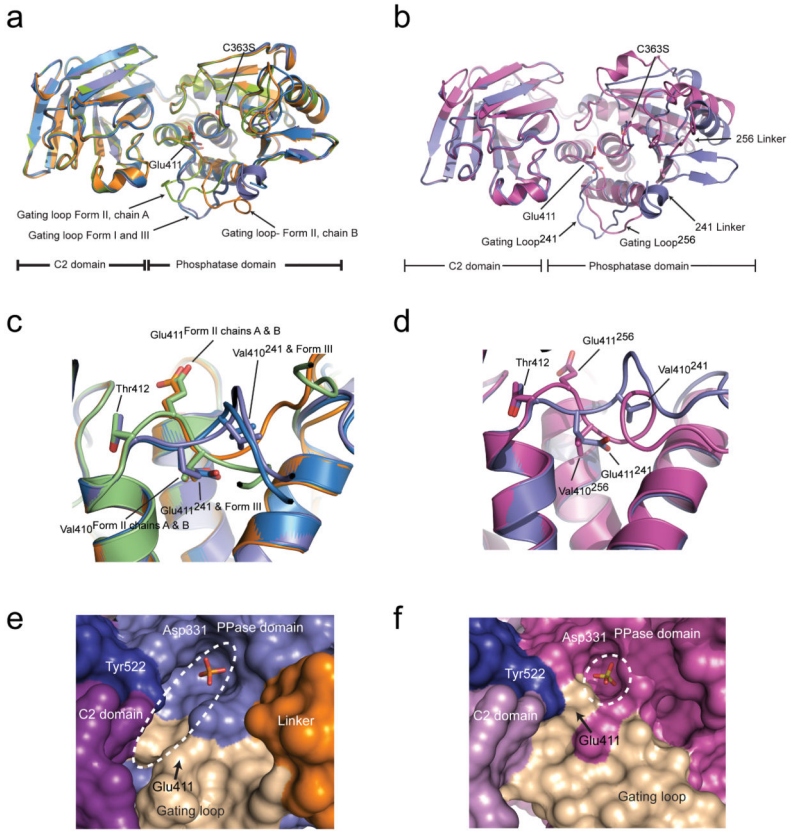

Figure 2.

Comparison of Ci-VSP intracellular domain structures reveals gating loop movements. (**a**) Superposed cartoon diagrams of Ci-VSP 241-576: Form I (slate); Form II, chain A (lime green); Form II, chain B (orange), and Form III (light blue). (**b**) Superposed cartoon diagrams of Ci-VSP 241 Form I (slate) and 256 (magenta). Active site C363S, Glu411, 241 linker, 256 linker, and gating loops are indicated. (**c**) Details gating loop and α456 pocket from Ci-VSP 241-576 Form I (slate); Form II, chain A (lime green); Form II, chain B (orange); and Form III (light blue). Val410, Glu411, and Thr412 are shown as sticks and are labeled. (**d**) Details gating loop and α456 pocket from: 241 Form I (slate) and 256 (magenta). V410, E411, and T412 are shown as sticks and are labeled. (**e**) Surface view of the Ci-VSP 241 (Form I) active site. Ci-VSP elements are colored: N-terminal linker (orange), phosphatase domain (slate), gating loop (tan), C2 domain (purple), 522 loop (dark blue). Active site phosphate is shown in sticks. Dashed oval indicates the open active site pocket. (**f**) Surface view of the Ci-VSP 256 active site. Ci-VSP elements are colored as follows: Phosphatase domain (magenta), gating loop (tan), C2 domain (pink), 522 loop (dark blue). Active site sulfate is shown in sticks. Dashed circle indicates the closed active site pocket. Note, colors of C2 domains differ in panels **e** and **f** to distinguish the 241 Form I, panel **e**, and 256, panel **f**, structures.

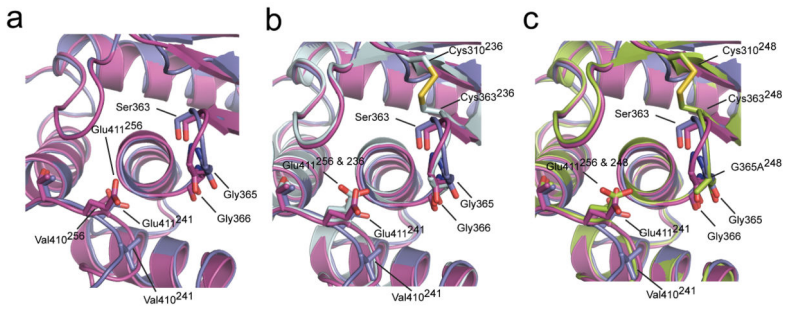

Figure 3.

Comparison of Ci-VSP active site P-loop conformations of (**a**) 241 (slate) and 256 (magenta); (**b**) 241 (slate) and 256 (magenta); and 236 (light blue) from Ref. 13; and (**c**) 241 (slate) and 256 (magenta); and 248 G365A (lime green) from Ref. 13. Key residues are labeled. Superscript indicates origin. Residues with common positions have no superscript.

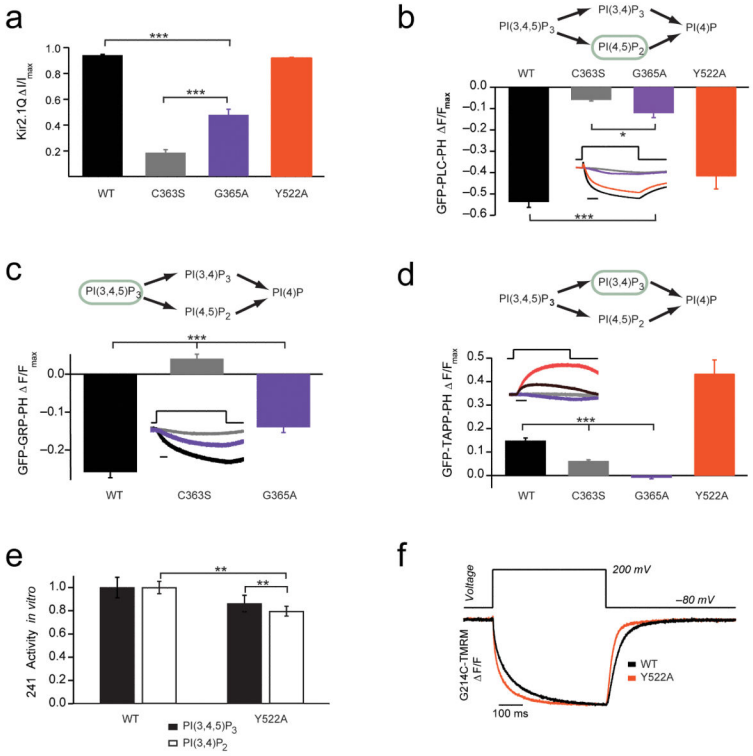

Figure 4.

Functional studies of Ci-VSP active site mutants. (**a**), Activity of full-length Ci-VSP in *Xenopus* oocytes measured using the $PI(4,5)P_2$ sensitive Kir2.1Q current. Average data for Kir2.1Q coexpressed with WT, C363S, G365A, Y522A in the G214C background. $\Delta I/I_{max}$ was calculated from the steady state current at holding potentials of −100 mV and +60 mV. (**b-d**) Activity of full-length Ci-VSP in *Xenopus* oocytes measured using: a $PI(4,5)P_2$ sensitive GFP-PLC-PH domain (**b**); a $PI(3,4,5)P_3$ sensitive GFP-GRP-PH domain (**c**); and a $PI(3,4)P_2$ sensitive GFP-TAPP-PH domain (**d**) Full-length Ci-VSP activity measured by Kir2.1Q co-expressed with WT, C363S, D400K and D400R in the G214C background. Error bars are Â± SEM, n=10-38. (**e**) *In vitro* malachite green activity assay with PS/$PI(3,4,5)P_3$ or PS/$PI(3,4)P_2$ vesicles and the cytosolic fragment of Ci-VSP 241 WT and Y522A. Error bars are ± SEM, n=3. (**f**) Representative TMRM fluorescence trace during a step from a holding potential of −80 mV to +200 mV for WT and Y522A. Traces normalized to the maximal fluorescence change. Voltage trace reports actual voltage recorded during acquisition. Asterisks indicate statistically significant differences using the student's t test, **p<0.01, ***p<0.001.

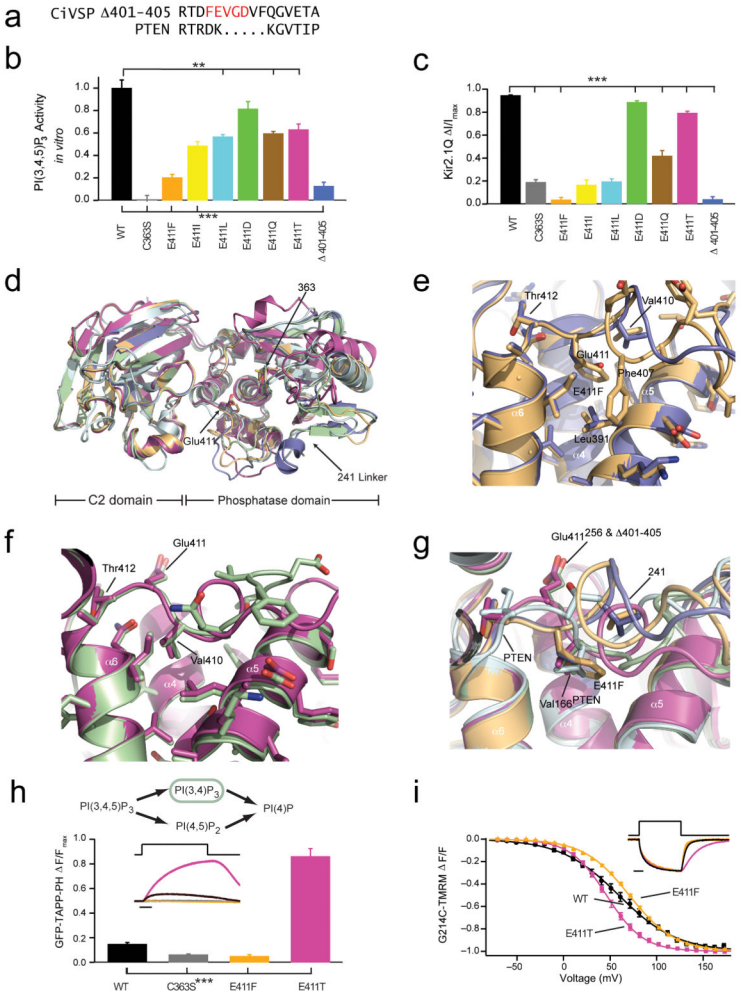

Figure 5.

Tests of gating loop functional importance. (**a**) Ci-VSP gating loop and PTEN TI loop sequences. Red indicates residues deleted in Ci-VSP Δ401-405. (**b**) PS/PI(3,4,5)P_3 vesicle malachite green activity assay with Ci-VSP 241 and indicated mutants. Error bars are ± SEM, n=3. (**c**) Full-length Ci-VSP activity measured by Kir2.1Q in *Xenopus* oocytes co-expressed with indicated mutants in the G214C background. (**d**) Cartoon diagrams of superposed Ci-VSP structures: 241 Form I (slate); 256 (magenta); 241 Δ401-405, (light green); and 256 E411F (light orange). (**e-g**) Comparison of α456 pocket and gating loop of 241 Form I (slate) and 256 E411F (light orange) (**e**), and 241 Δ401-405 (light green) and 256 (magenta) (**f**), and 241 Form I (slate), 241 Δ401-405 (light green); 256 (magenta); and PTEN (cyan) (**g**). (**h**) Activity of full-length Ci-VSP in *Xenopus* oocytes measured using GFP-TAPP-PH. Average ΔF/F for WT, C363S, E411F and E411T in the G214C background. Insets show fluorescence traces for TAPP data normalized to C363S to control for native Xl-VSP. (**i**) Normalized F-Vs of full-length Ci-VSP. Data are fit to single Boltzmann equations. (WT $V_{1/2}$= 59 ± 1, slope= 31 ± 1; E411F $V_{1/2}$= 70.6 ± 0.4, slope= 24.5 ± 0.4; E411T $V_{1/2}$= 46.1 ± 0.2, slope= 19.7 ± 0.2). Error bars are ± SEM, n=9-15.

Asterisks indicate statistically significant differences using the student's t test, **p<0.01, ***p<0.001.

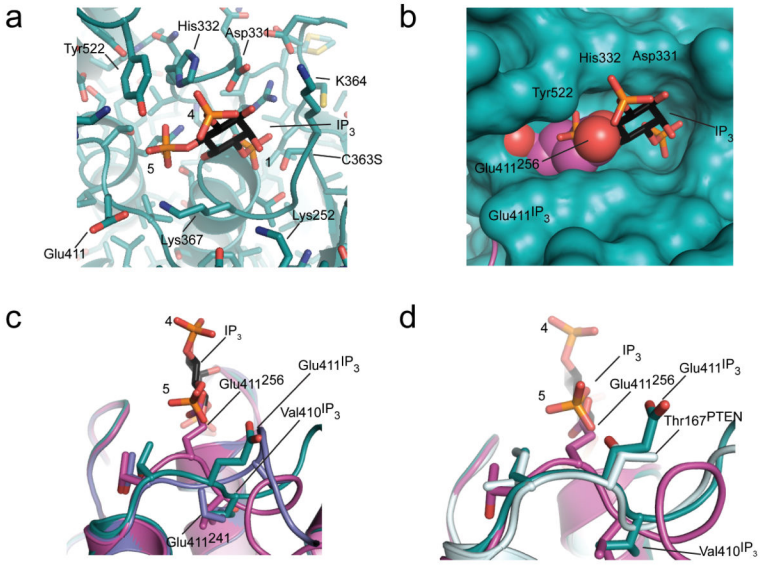

Figure 6.

Structure of a Ci-VSP-IP_3 complex. (**a**) Ci-VSP-IP_3 complex active site. Ci-VSP residues and IP_3 phosphate positions are indicated. (**b**) Surface representation of Ci-VSP-IP_3 complex active site. IP_3 and gating loop are shown as sticks. Glu411 from the 256 structure is shown as magenta and red spheres. Active site residues are labeled. (**c-d**) Comparison of active sites and gating loop Glu411 element from 241 Form I, 256, and the IP_3 complex colored slate, magenta, and dark teal, respectively (**c**) and PTEN, 256, the IP_3 complex, and colored light blue, magenta, and dark teal, respectively (**d**). Superscripts denote the relevant structure for the labeled elements.

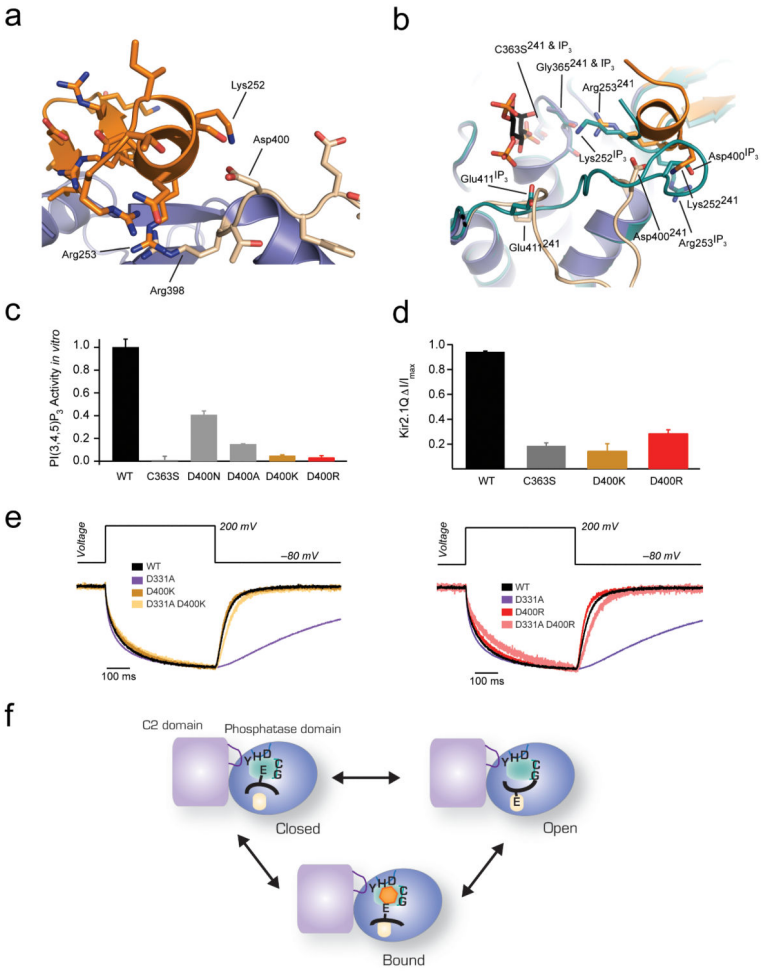

Figure 7.

Ci-VSP linker-gating loop coupling. (**a**) Cartoon diagram of 241 Form I linker-gating loop region. Phosphatase domain, linker, and gating loop are colored slate, orange, and tan, respectively. Sidechains are shown as sticks. Select residues labeled. (**b**) Comparison of linker and gating loops from the 241 Form I (slate) and IP_3 complex structures (teal). Key residues and IP_3 are shown as sticks. Superscript indicates origin. (**c**) Malachite green assay with PS-PI(3,4,5)P_3 vesicles for Ci-VSP 241 and indicated mutants. Error bars are ± SEM, n=3. (**d**) Full-length Ci VSP activity measured by Kir2.1Q co-expressed with WT, C363S, D400K and D400R in the G214C background. Error bars are ± SEM, n=10-38. (**e**) Representative TMRM fluorescence trace during a step from a −80 mV holding potential to +200 mV for labeled G214C and indicated mutants in the G241C background. Traces normalized to the maximal fluorescence change. Voltage trace reports actual voltage recorded during acquisition. (**f**) Cartoon diagram indicating the three positions of the gating loop switch segment. Phosphatase (blue oval) and C2 domain (purple square) are indicated. Active site residues Y522, H332, D331, C363, G365 and gating loop E411 are depicted. Phosphatase domain green and grey elements indicate the active site and α456 pocket, respectively.

Table 1

X-ray Data collection and Refinement Statistics

Data Collection	241-576 (C363S) (Form I)	241-576 (C363S) (Form II)	241-576 (C363S) (Form III)	241-576 (Δ401-405) (C363S)	256-576 (C363S)	256-576 (E411F)	241-576 (C363S) + IP_3
Resolution (Å)	100-1.10(1.12-1.10)	100-1.30 (1.33-1.30)	100-1.50 (1.54-1.50)	100-1.72 (1.78-1.72)	100-1.60 (1.65-1.60)	100-1.95 (2.02-1.95)	100-1.85 (1.92-1.85)
Space group	$P2_1$	$P2_1$	P_1	$P2_1$	P_2	$P2_12_12_1$	$P2_1$
Cell Dimensions							
a, b, c, (Å)	50.967 85.706 84.327	50.746 80.375 83.637	50.863 83.863 83.604	50.562 76.804 84.007	50.849 38.605 89.832	50.980 76.590 84.950	50.665 79.852 87.927
α, β, γ(°)	90 90.964 90	90 93.119 90	86.552 89.548 89.375	90 92.729 90	90 103.992 90	90 90 90	90 92.440 90
R_{sym} (%)	5.4 (47.5)	8.4 (58.4)	5.5 (29.0)	11.6 (74.0)	7.0 (67.2)	11.2 (38.3)	11.1 (66.0)
I/σI	21.4 (2.2)	26.3 (3.5)	15.3 (2.4)	14.4 (2.0)	18.1 (2.4)	13.6 (3.1)	17.2 (3.4)
Total Reflections	2445254	4385060	3194799	1081730	606240	532266	1952687
Unique Reflections	291443	153889	176659	68903	43750	24720	59840
Completeness (%)	99.6 (96.9)	94.1 (90.1)	80.5 (83.1)	100.0 (100.0)	97.7 (82.2)	99.9 (99.8)	99.9 (99.6)
Redundancy	4.3 (2.9)	12.5 (7.0)	2.6 (1.4)	6.9 (3.7)	5.8 (4.1)	5.6 (3.5)	7.4 (7.3)
Refinement							
Resolution (Å)	84.4-1.10	83.6-1.30	83.8-1.60	84.0-1.72	87.2-1.65	56.9-1.95	87.9-1.85
No. reflections	276406	146117	138269	64627	38746	21796	56716
R_{work}/R_{free}	14.0/16.1	14.0/17.6	25.6/29.8	18.5/22.2	17.7/21.0	22.1/26.1	18.1/22.2
Number of atoms							
Protein	5669	5589	10671	5288	2601	2359	5410
Ligand/ion	20	20	45	10	34	20	96
Water	985	875	1169	506	222	217	676
B-factor							
Protein	21.1	20.3	24.0	25.3	31.1	17.7	21.1
Ligand/ion	21.1	14.6	34.2	25.5	41.2	37.3	52.6
Water	38.1	39.2	31.7	36.4	51.1	25.5	33.1
RMS Deviations							

Data Collection	241-576 (C363S) (Form I)	241-576 (C363S) (Form II)	241-576 (C363S) (Form III)	241-576 (Δ401-405) (C363S)	256-576 (C363S)	256-576 (E411F)	241-576 (C363S) + IP_3
Bond lengths (Å)	0.011	0.01	0.006	0.008	0.008	0.007	0.008
Bond angles (°)	1.47	1.35	0.956	1.11	1.08	1.07	1.22
Ramachandran Plot							
Favored region (%)	95.8	96.2	95.0	94.3	95.2	95.2	95.3
Allowed region (%)	3.5	3.3	3.9	4.8	3.6	3.6	3.1

* Values in parentheses are those for the outmost resolution shell

** 5% of randomly selected reflections were used for Rfree monitoring during refinement